

SDC
SOLENOIDAL DETECTOR NOTES

SI BARREL LAYER RADII

August 11, 1992

Mark Strovink
Lawrence Berkeley Laboratory

Si Barrel Layer Radii
M. Strovink (LBL)

1. Introduction.

The nominal radii of the SDC Si barrel layers (90, 120, 180, 210, 240, 270, 330, and 360 mm as in the TDR) need to be reduced slightly to ensure adequate azimuthal overlap of stereo strips. These radii should be fixed soon so that further optimization of the Si disk layout may proceed, and more refined mechanical engineering may continue.

2. Summary.

The conclusion of this study is that the above radii should be reduced by 3, 4, 6, 7, 7, 8, 10, and 11 mm, respectively (about 3%). Approximately half of the reduction is to close azimuthal cracks in the acceptance; the other half is to achieve a 0.5 mm overlap for use in aligning detectors within a given layer.

3. Assumptions.

The number of ladders around the azimuth is assumed to be 18, 24, 36, 42, 48, 54, 66, and 72, respectively, for the eight barrel layers as in the TDR. These numbers maintain a simple relationship to the nominal radii because the active width of a detector is approximately π cm. By "detector radius" we mean the distance from the beam axis to the center of mass of the detector.

It should be noted that choosing nominal radii of 80, 120, 160, 200, 240, 280, 320, and 360 mm -- same as at present, except that the inner radius would be reduced by 10 mm and the layers would be uniformly spaced -- would result in numbers of ladders around the azimuth that are divisible by eight rather than six. Because the rest of the SDC detector is organized in octants, this would simplify the trigger and analysis logic. However, the radiation damage to the inner Si layer would be accelerated by 27%.

When a radial track is incident on the center (symmetry point) of a physical detector, it is assumed to make an angle, projected on the x-y plane, of 6 deg with the detector normal. This angle was chosen, as part of the general SDC Si detector design, to enable efficient and timely collection of electrons and holes under the influence of crossed electric and magnetic fields.

For the geometry of the barrel Si detectors, the exceptionally clear Japanese drawings 3S0418-3 and -4 are used. On the axial side, the active area is a $58.8 \times 32.0 \text{ mm}^2$ rectangle. On the stereo side, it is a parallelogram obtained by displacing each short rectangular end by $\pm 0.294 \text{ mm}$. The resulting stereo angle is $\arctan(2 \times 0.294 / 58.8) = 9.999666 \text{ mrad}$. Both these rectangular and parallelographic shapes are centered on the physical detector ($34.1 \times 60 \text{ mm}^2$).

For the geometry of the Si ladders, it is assumed that detectors are bonded end to end with no offset, and that the direction of the wire bonds is axial.

For stiff tracks, it is assumed that no geometrical inefficiency arising from inadequate azimuthal overlap can be allowed. Here "stiff" is taken to mean $P_t > 20 \text{ GeV}/c$, approximately the lower P_t limit for multilepton triggers in SDC. Because of the 6 deg shingling of the barrel detectors, such inefficiency would

be charge asymmetric, without the possibility of cancellation by reversing the magnetic field direction. For reference, the irreducible geometrical inefficiency from lack of axial overlap is $(2 \times 600 \text{ um} / 60 \text{ mm}) = 2\%$ within the ladders (more outside).

Beyond eliminating geometric inefficiency, it is assumed that at least 0.5 mm (10 strips) of azimuthal overlap are needed for relative alignment of detectors in a single layer. Because the nominally axial strips in reality will make a finite angle with the detector axis, tracks used in such alignment studies must be measured in all 3 dimensions to make possible the necessary z-dependent corrections. Therefore, 10-strip overlap must be achieved for the part of the ladder in which both axial and stereo strips are active.

4. Active ladder geometry.

With these assumptions, half a ladder is drawn to (unspecified) scale in Fig. 1, showing the boundaries of the physical, active axial strip, and active stereo strip regions. Figure 2 displays the area in which both axial and stereo strips are active. It consists of a parallelogram separated by 1.2 mm from a six-sided figure. The 10 mrad angle between two pairs of the six sides is barely discernable.

5. Geometry of barrel layer 1.

Figure 3 is an isometric view of two ladder halves with radius of 90 mm and angular separation of 20 deg, appropriate for the innermost barrel layer. (For arcane reasons, the beam axis is vertical.) In order to measure inefficiency due to inadequate azimuthal overlap, we need a perspective view with the eye at the origin, focused on the gap between the ladders. That is supplied by Fig. 4, where it is seen that significant inefficiency is present in the crack between the (bottom) detectors at the end that is not read out.

A $Pt=20 \text{ GeV}/c$ particle, curved with radius $R=33.3 \text{ m}$ in the 2T field, crosses the surface $r=90 \text{ mm}$ as would a straight track with distance of closest approach $b = r^2/2R$ with the axis. In this example, b is only 0.12 mm. Figure 5 confirms that the azimuthal overlap is not perceptibly different when viewed from this point of closest approach, compared to the view from the origin.

Figure 6 is the same view with the detectors at 88 rather than 90 mm radius. Here the overlap is positive at the top, and positive or near zero at the bottom.

Figure 7 is the same as Fig. 6 except the detectors are at 87 mm radius. The azimuthal overlap is significant at all points along the crack.

We conclude that reducing the inner barrel layer radius from 90 to 88 mm is sufficient to cause its azimuthal crack to (nearly) vanish.

6. Geometry of barrel layers 8 and 3.

Figures 8 and 9 are the same as Figs. 3 and 4, except that layer 8 is shown. At its nominal radius of 360 mm, again at $Pt=20 \text{ GeV}/c$, the distance of closest approach to the beam axis of the equivalent straight track is 1.94 mm rather than 0.12 mm (factor of 16). Viewed in Fig. 10 from this point of closest approach, compared to the view from the origin, the crack is larger by an amount that is barely perceptible. Thus the effect of $Pt=20 \text{ GeV}/c$ track curvature is almost negligible even at this largest radius.

Figure 11 shows that reduction of the layer 8 radius from 360 to 355 mm is enough to close the crack.

Figure 12 is analogous to Fig. 11 but it refers to layer 3. Here it is seen that reduction of the layer 3 radius from 180 to 177 mm closes layer 3's azimuthal crack.

7. Azimuthal overlap for alignment.

To achieve an additional 0.5 mm of azimuthal overlap for alignment purposes, one needs to reduce the detector radius by the fraction $0.5 \text{ mm} / 31 \text{ mm} = 1.6\%$.

8. Summary of changes to barrel radii.

The changes in barrel radii indicated by this study are the following (all distances in mm):

Layer	Nominal radius	Reduction to close crack	Reduction for 500 μ overlap	New radius (rounded)
1	90	2	1.4	87
2	120	2.3*	1.9	116
3	180	3	2.9	174
4	210	3.3*	3.4	203
5	240	3.7*	3.8	233
6	270	4*	4.3	262
7	330	4.7*	5.3	320
8	360	5	5.8	349

*interpolated value

As Hans Ziock has already pointed out in private conversation, the necessary reduction in radius is about 3% for all layers.

SDC Barrel Ladder

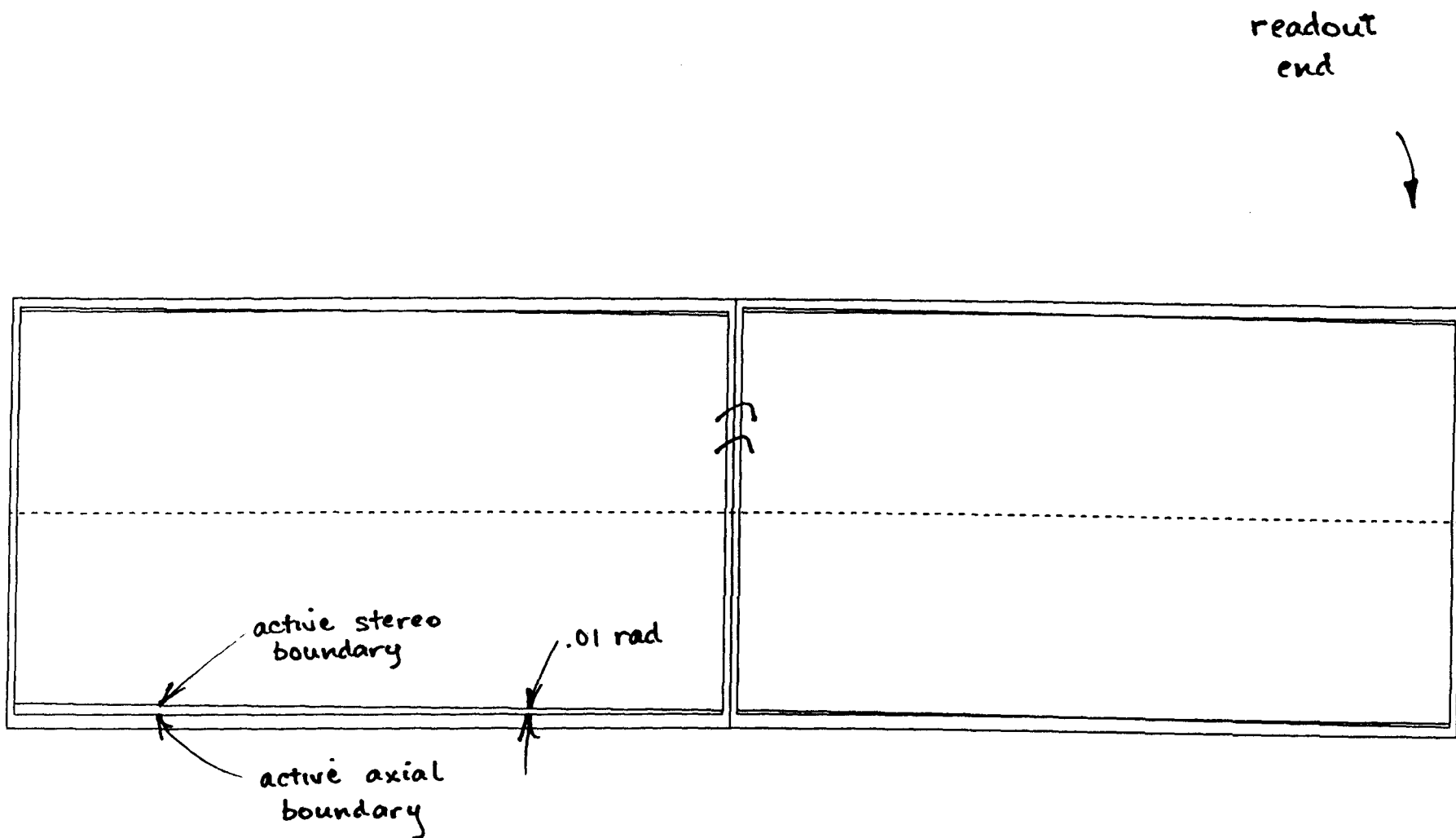


FIG. 1

SDC Barrel Ladder

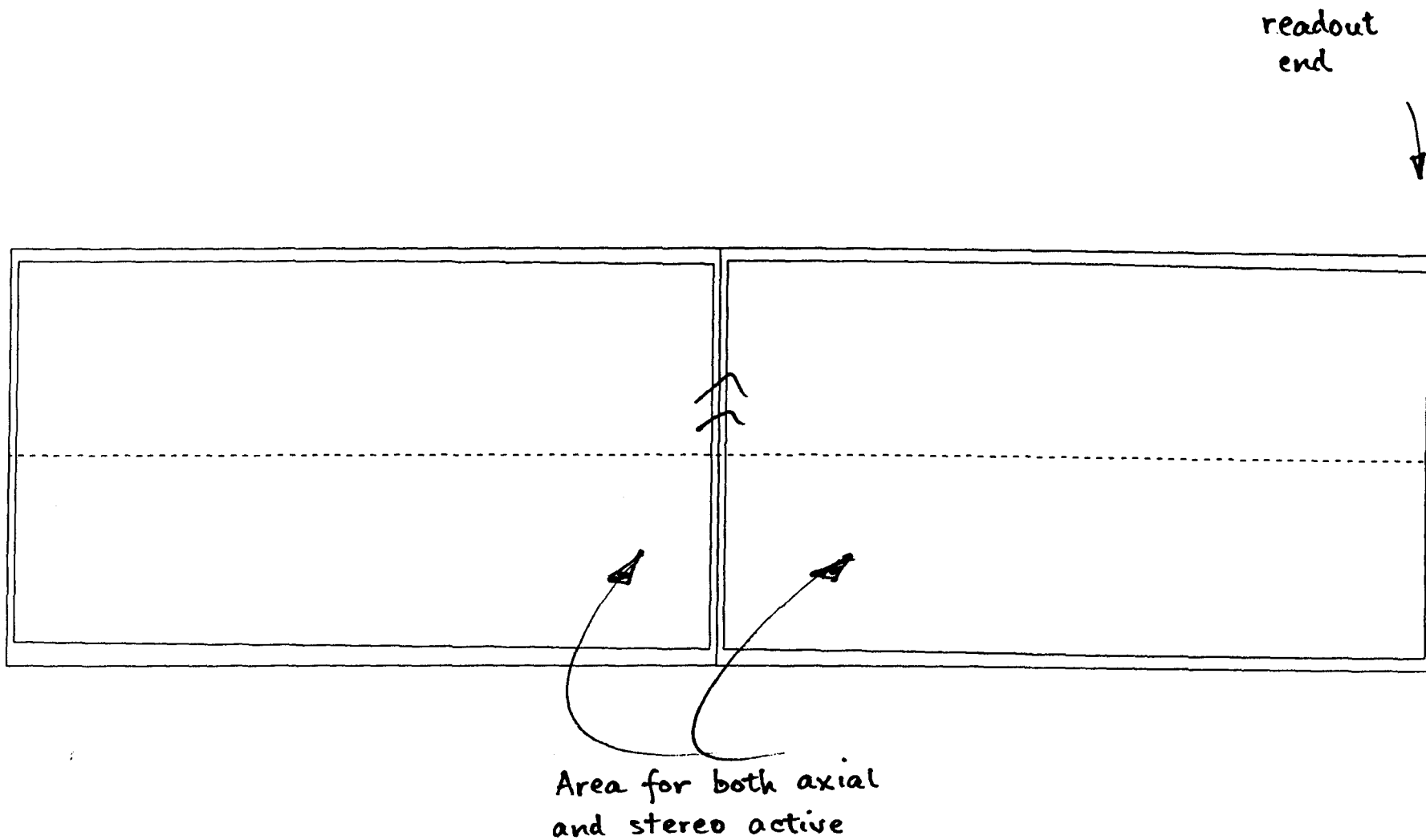
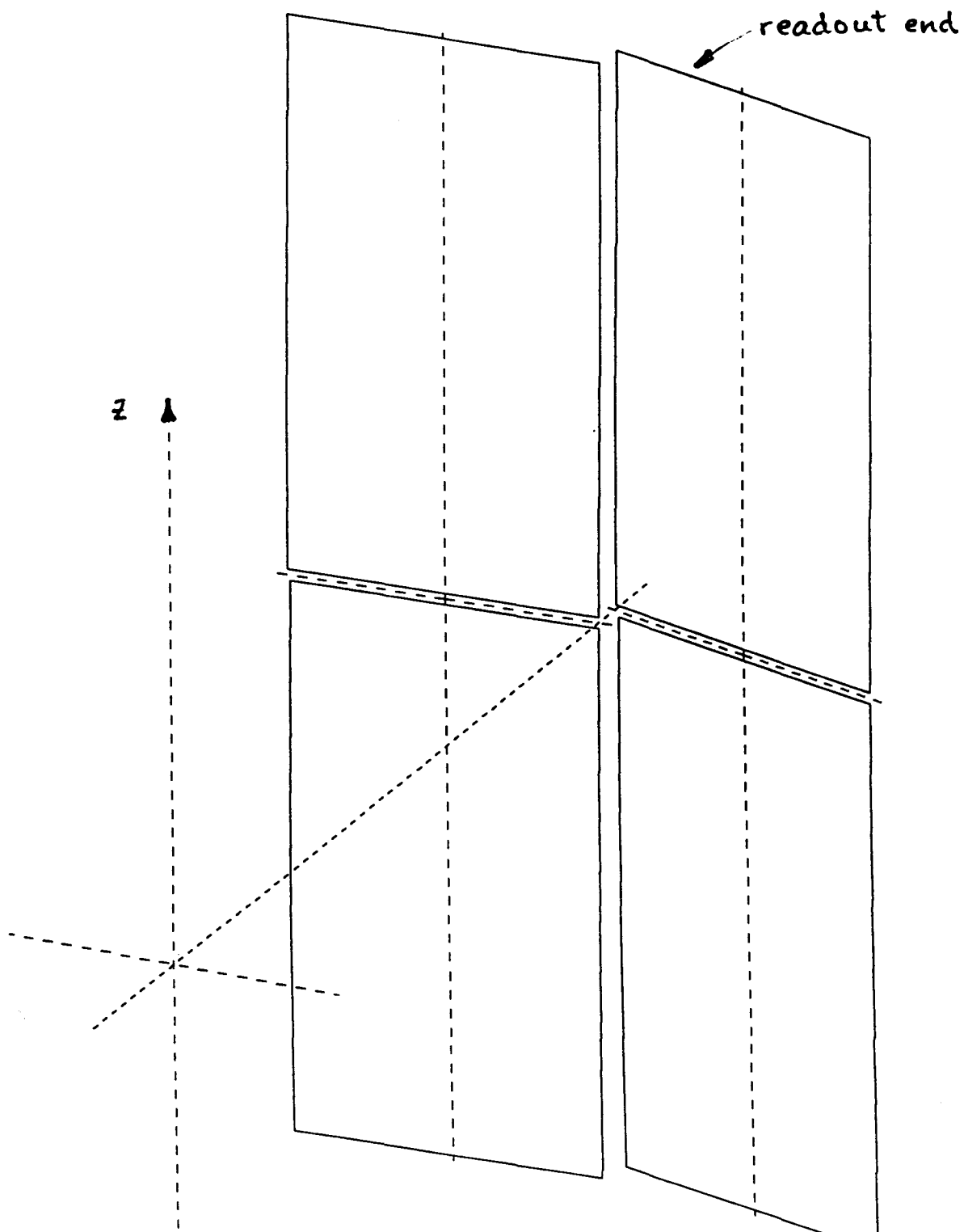


FIG. 2

isometric view

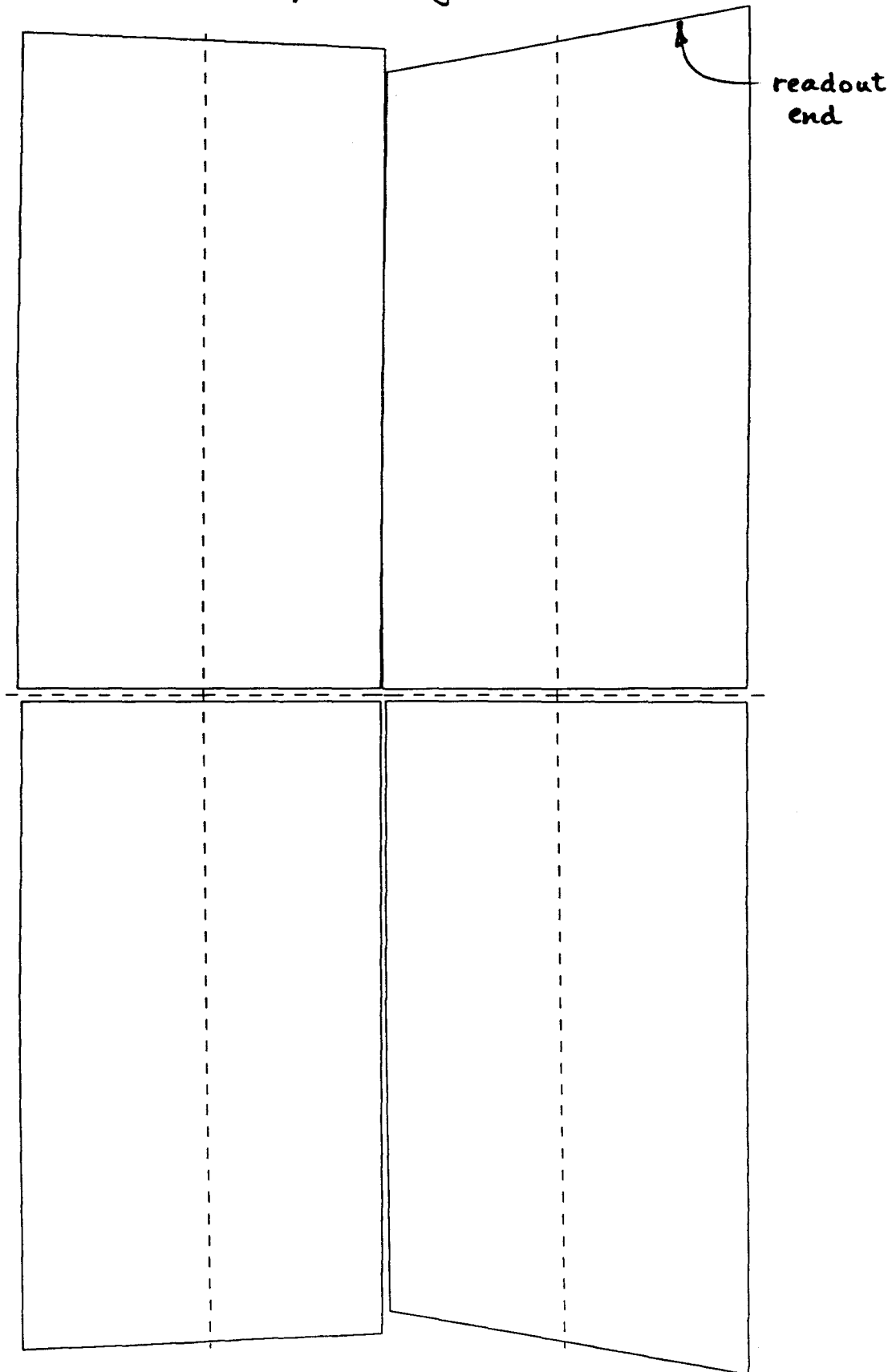


Layer 1 (18 around)

$$r = 90$$

FIG. 3

perspective view -
eye at origin

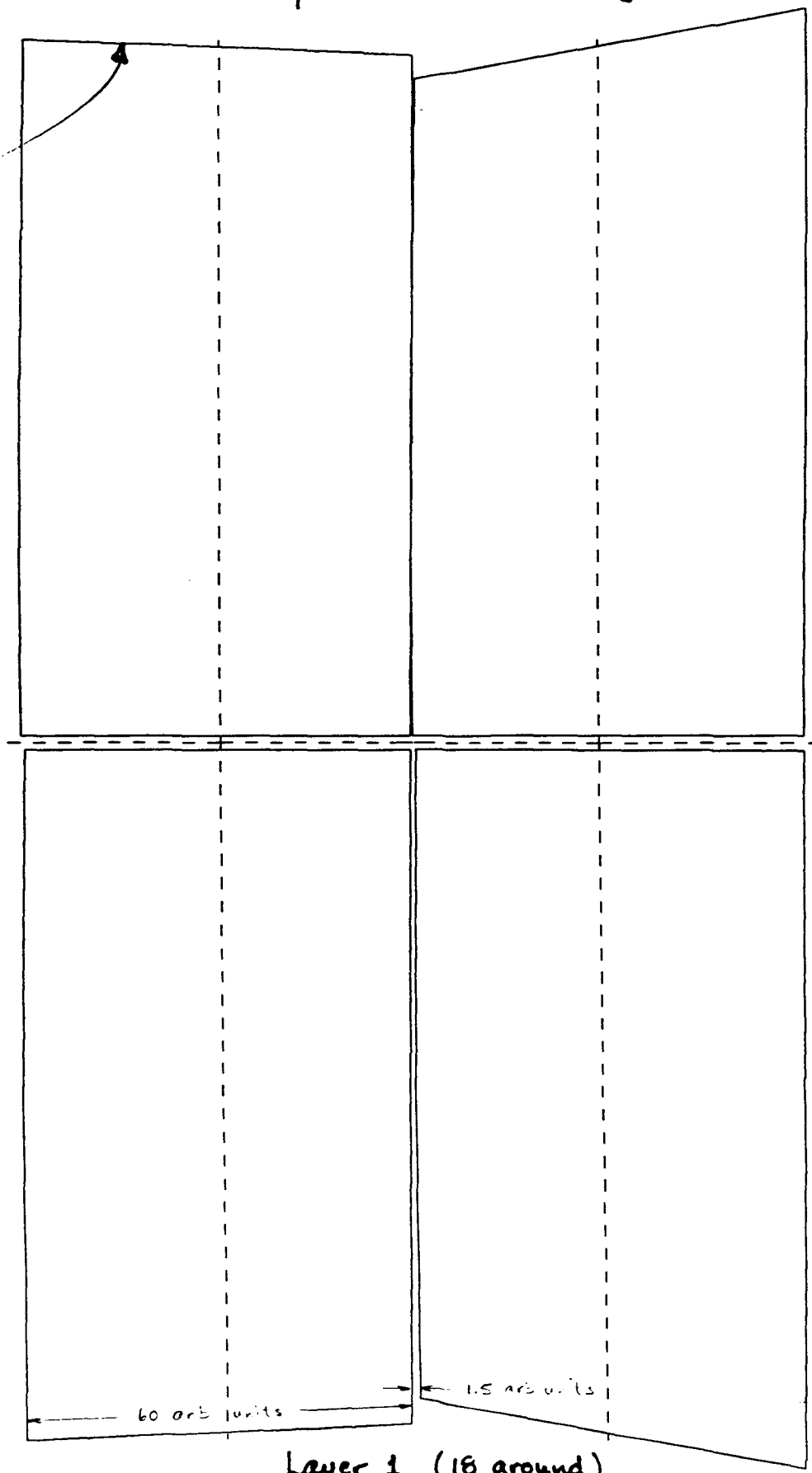


Layer 1 (18 around)

$r = 90$ FIG. 4

perspective view -
eye at 0.12 mm to right of origin

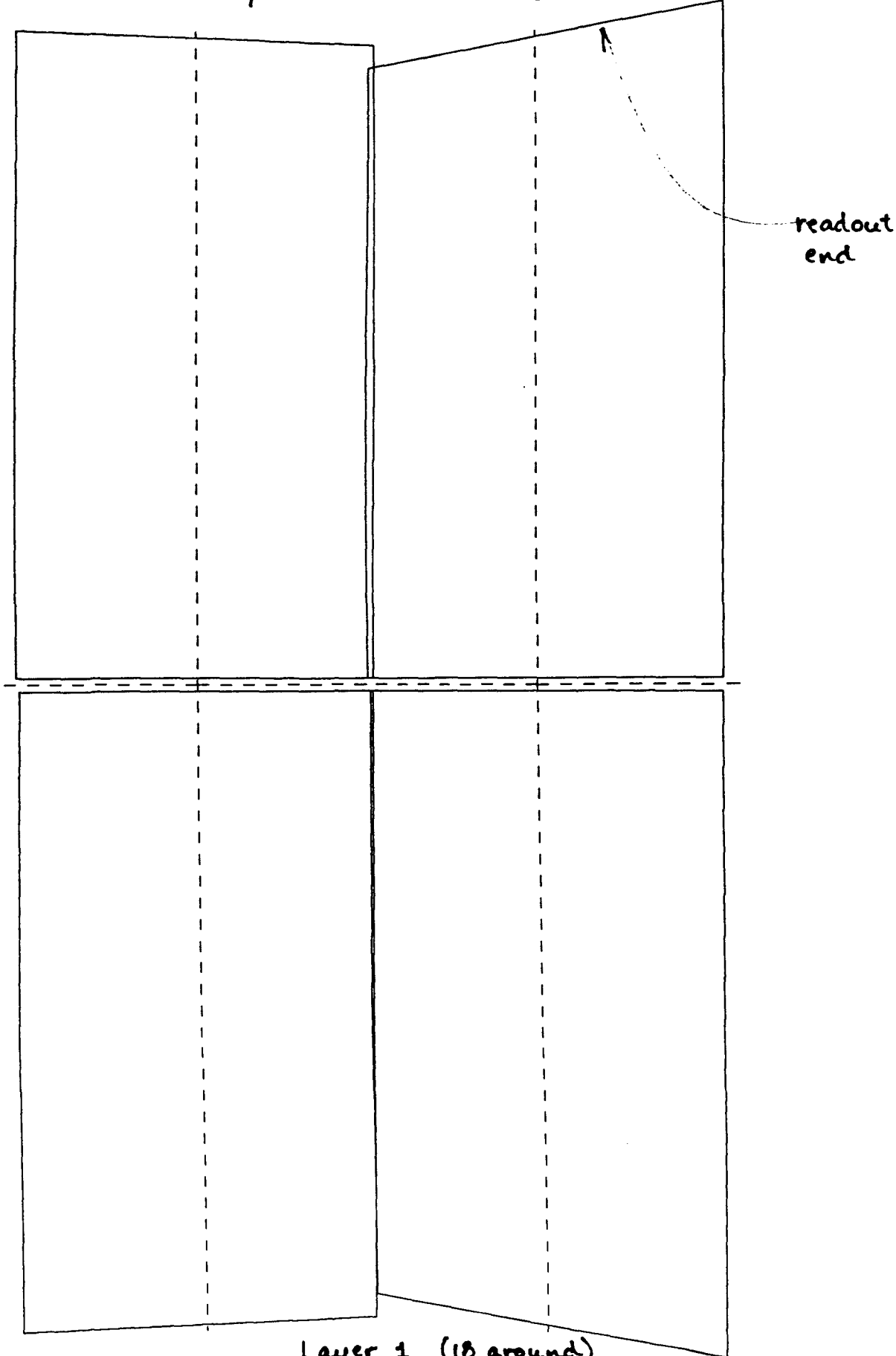
readout
end



Layer 1 (18 around)

$r = 90$ FIG. 5

perspective view -
eye at 0.12 mm to right of origin



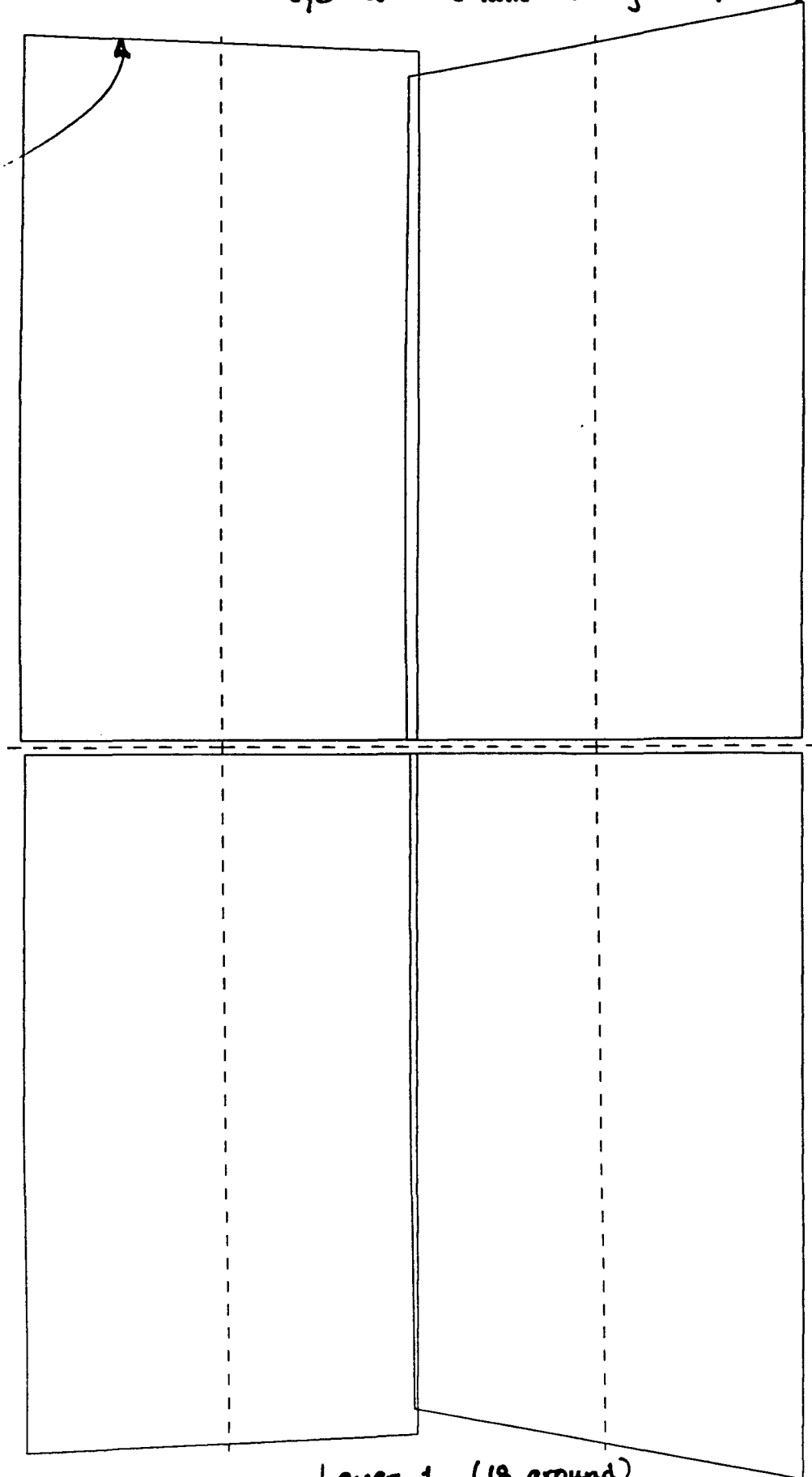
Layer 1 (18 around)

r = 88

FIG. 6

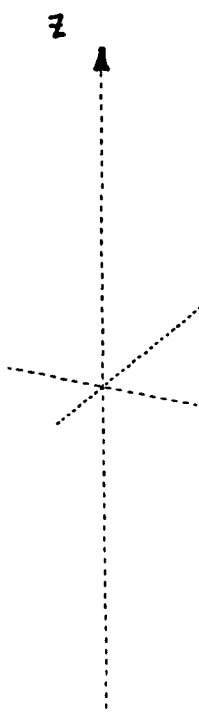
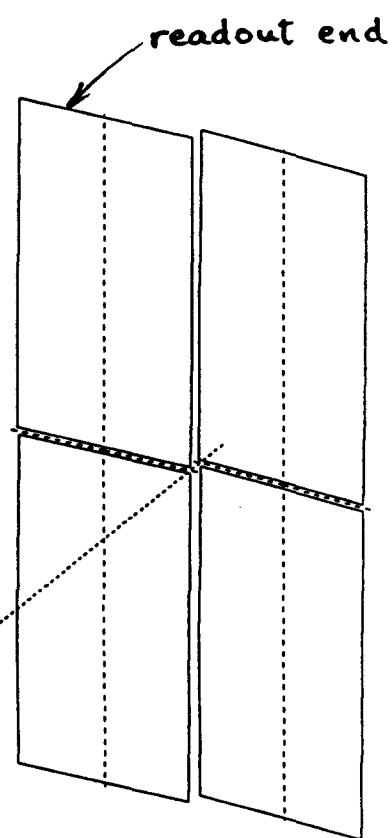
perspective view -
eye at 6.12 mm to right of origin

readout
end



Layer 1 (18 around)
 $r = 27$ FIG. 7

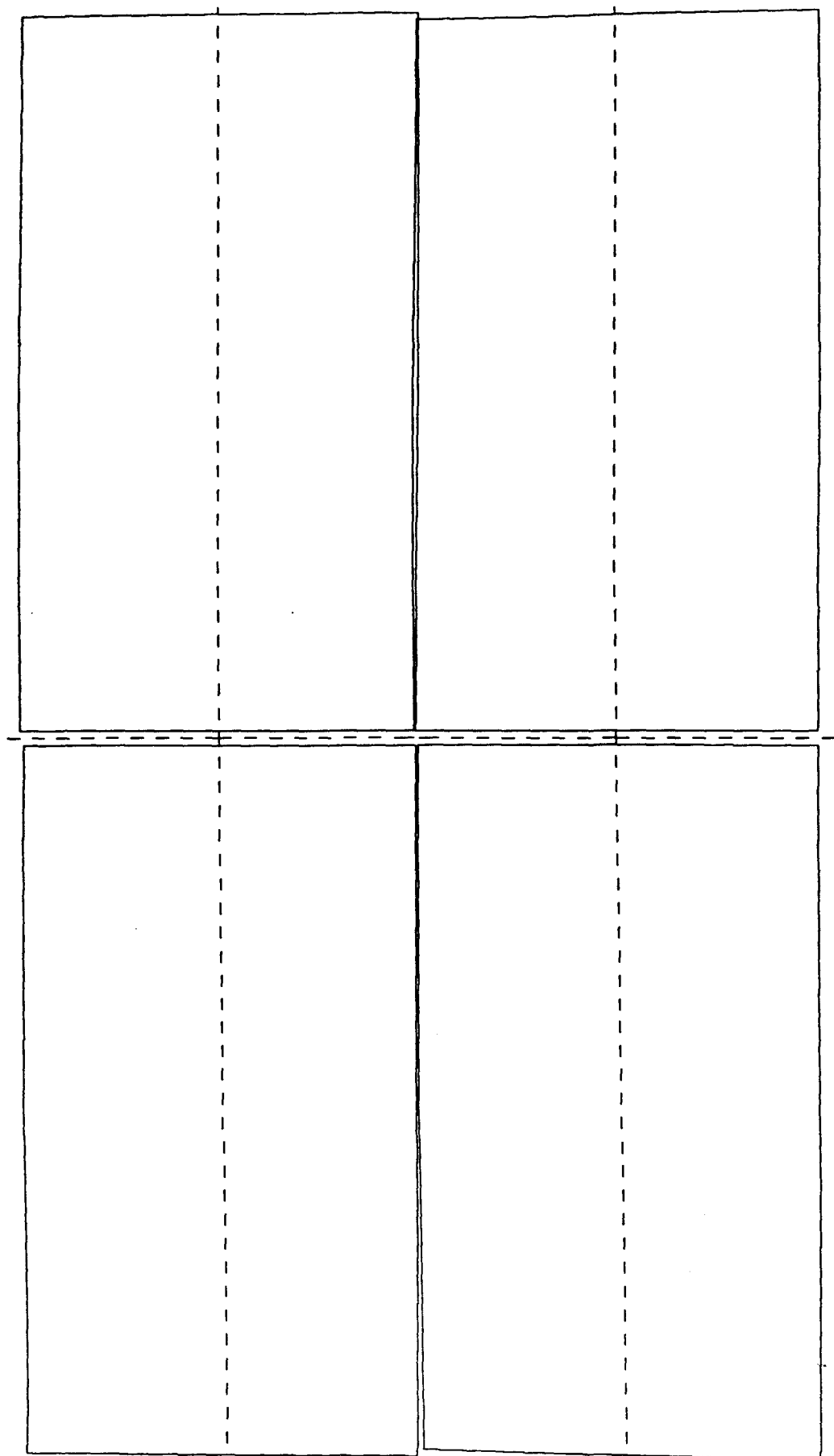
isometric view



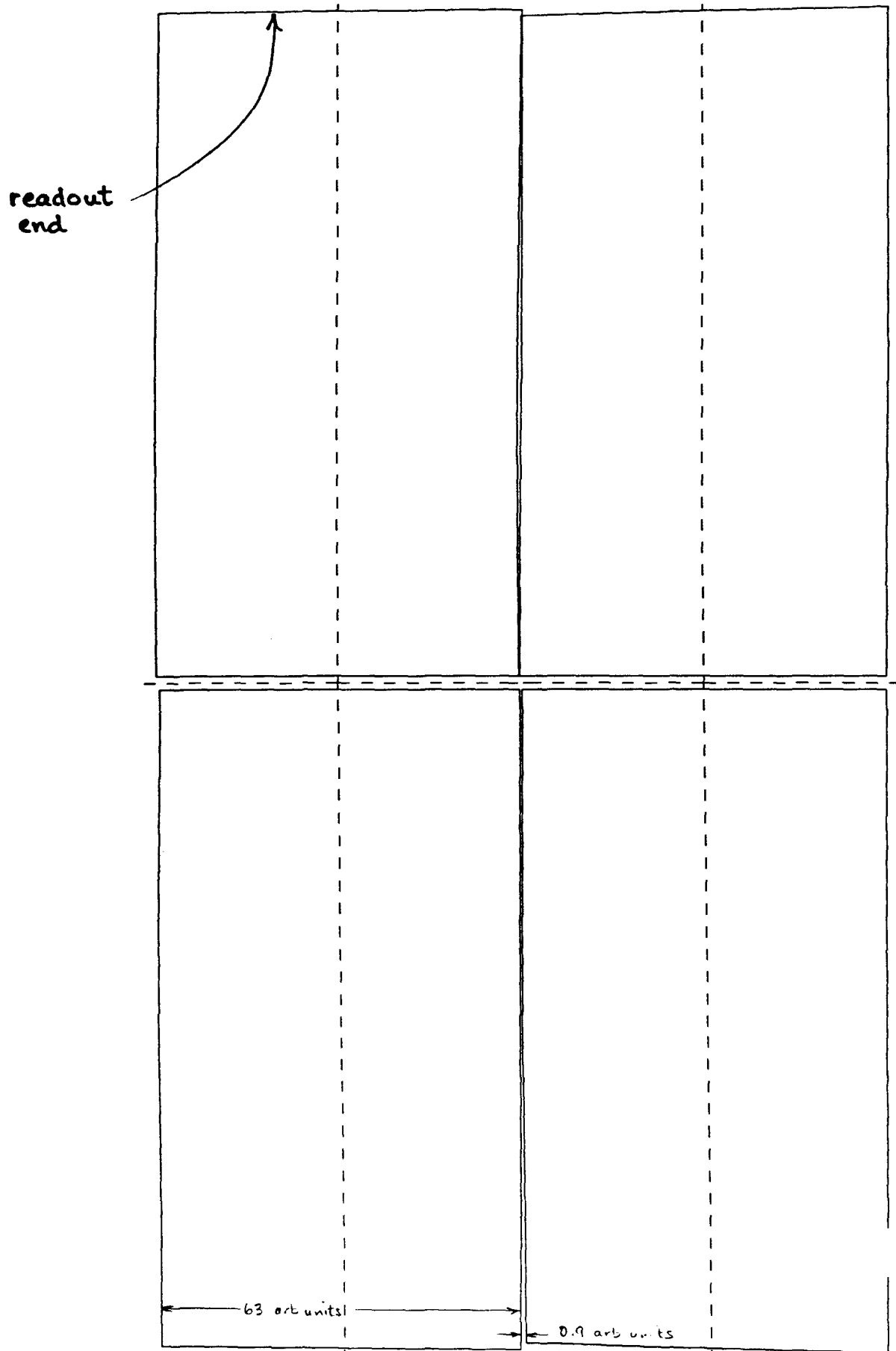
Layer 8 (72 around)
 $r = 360$

FIG. 8

perspective view -
eye at origin



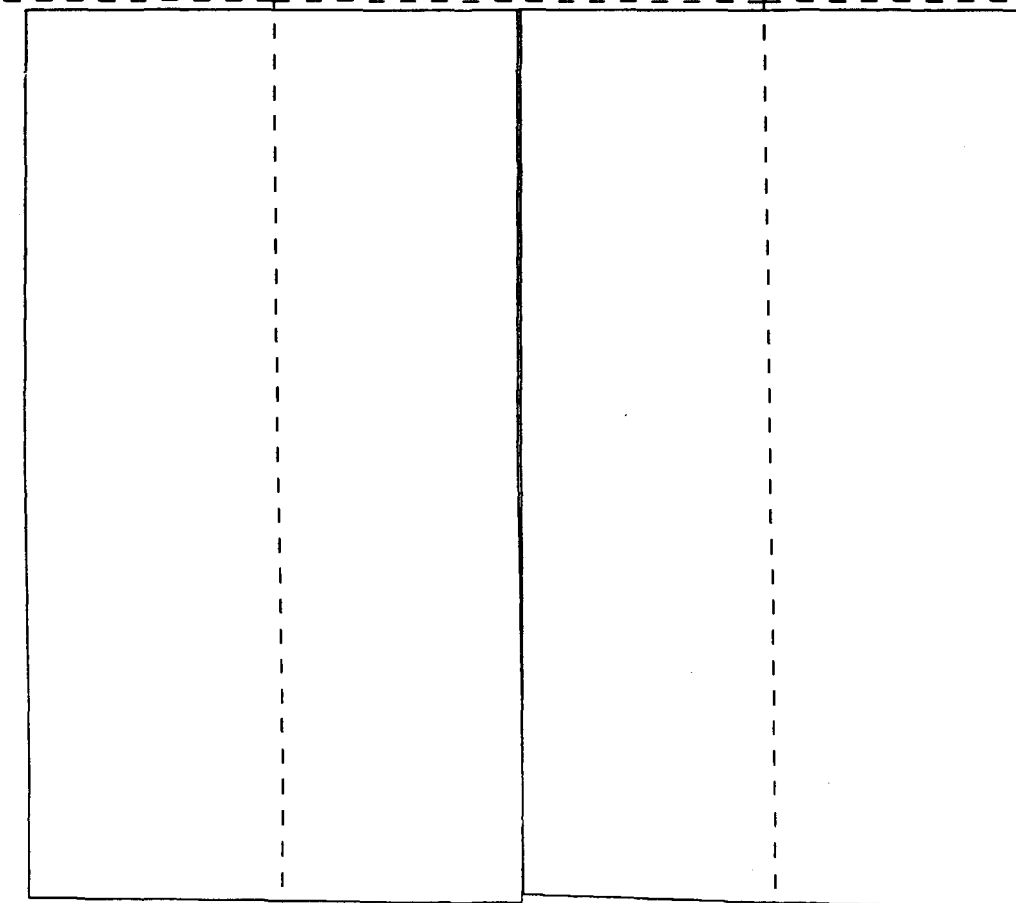
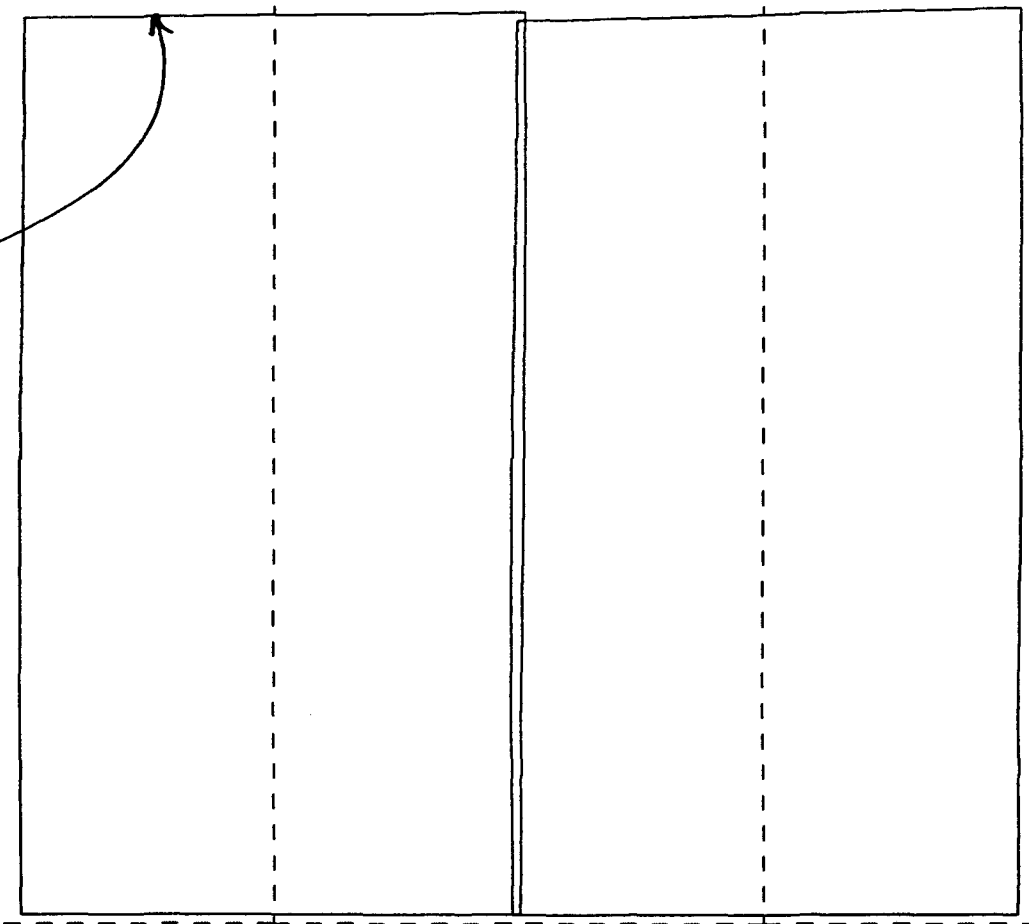
perspective view -
eye at 1.94 mm to right of origin



Layer 8 (72 around) : $r = 360$ FIG. 10

perspective view -
eye at 1.94 mm to right of origin

readout
end



perspective view -
eye at 0.48 mm to right of origin

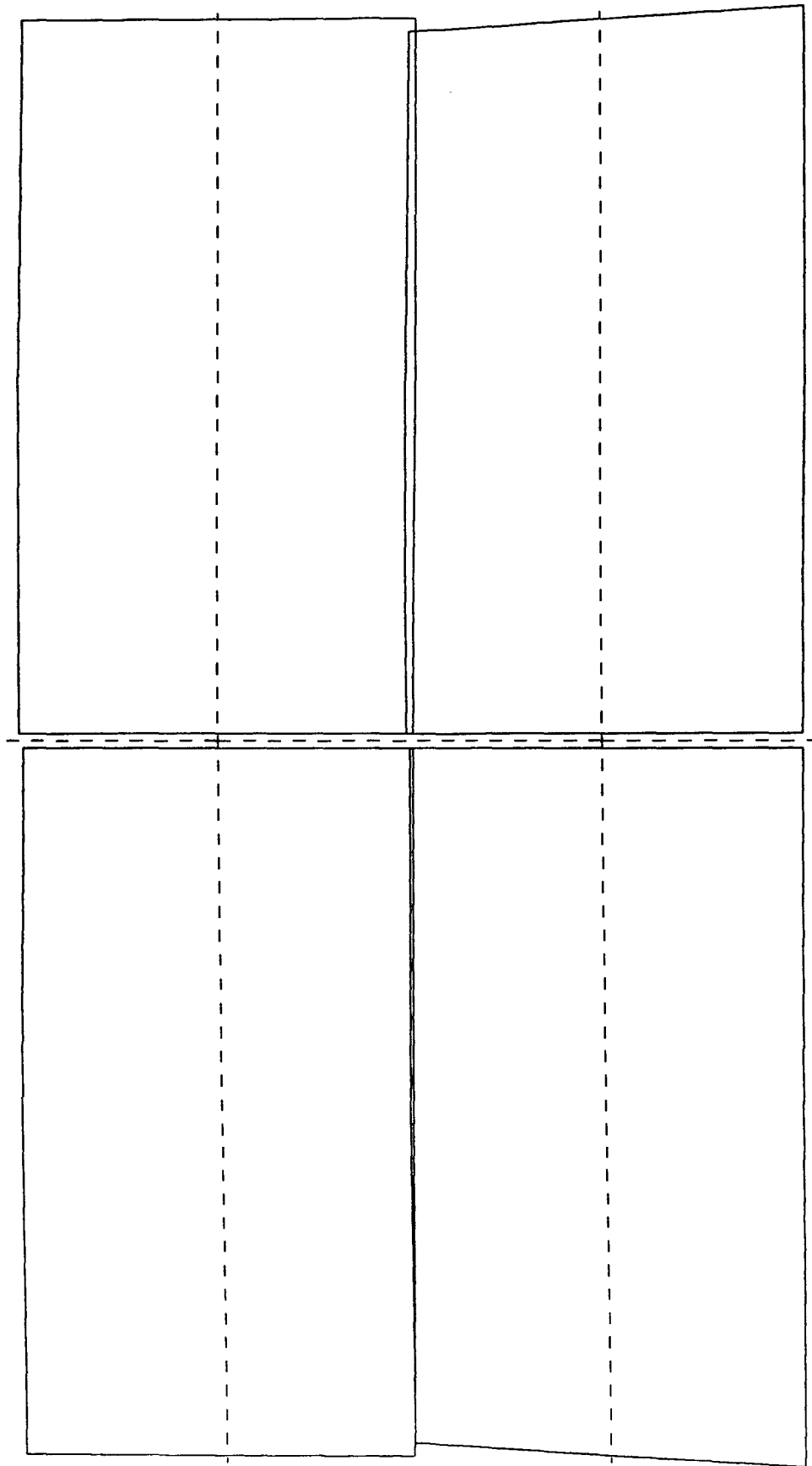


FIG. 12 Layer 3 (36 around) : $r = 177$